Journal of Physics: Conference Series **133** (2008) 012015 doi:10.1088/1742-6596/133/1/012015

Channeling of protons through carbon nanotubes

D. Borka[1], D. J. Mowbray[2], Z. L. Mišković[2], S. Petrović[1] and N. Nešković[1]

[1]Laboratory of Physics (010), Vinča Institute of Nuclear Sciences, P. O. Box 522, 11001 Belgrade, Serbia
[2]Department of Applied Mathematics, University of Waterloo, Waterloo, Ontario, Canada N2L3G1

E-mail: dusborka@vin.bg.ac.yu

Abstract. We investigate how dynamic polarization of carbon valence electrons influences both the angular and spatial distributions of protons channeled in a (11, 9) single-wall carbon nanotube placed in vacuum and in different dielectric media. Proton speeds between 3 and 10 a.u., corresponding to energies of 0.223 and 2.49 MeV, are chosen with the nanotube length varied between 0.1 and 1 μm. In all performed calculations we describe the interaction between proton and carbon atoms on the nanotube wall using the Doyle-Turner potential. The image force on a proton is calculated using a two-dimensional hydrodynamic model for the dynamic response of the nanotube valence electrons and the dielectric media surrounding the nanotube. The angular distributions of channeled protons are generated using a computer simulation method which solves the proton equations of motion in the transverse plane numerically. The best level of ordering and straightening of carbon nanotube arrays is often achieved when they are grown in a dielectric matrix. Consequently, we investigate here how the dynamic polarization of carbon valence electrons in the presence of various surrounding dielectric media affects the angular distributions of protons channeled through (11, 9) single-wall carbon nanotubes. Our analysis shows that the inclusion of the image interaction, gives rise to a number of rainbow maxima in the corresponding angular and spatial distribution. Our analysis shows that the presence of dielectric media surrounding the nanotube influences the positions and appearance of rainbows in the corresponding angular and spatial distributions. In addition, we analyze the possibility of production of nano-sized beams by carbon nanotubes.

1. Introduction

Theoreticians continue to explore possible applications of ion channeling through nanotubes [1, 2, 3], beginning with those based on the *angular* distributions of channeled ions, e.g., for the purpose of deflecting ion beams in accelerators [4] or determining some structural details of the short nanotubes using the rainbow effect [5, 6, 7, 8]. Theoretical studies of the *spatial* distributions of channeled ions have demonstrated the possibility of creating nanosized ion beams, which could find interesting applications in biomedical research and for materials modification [4, 9]. An additional application of ion channeling through nanotubes based on the *spatial* distributions remains to be investigated in the context of extending the classical use of ion channeling for materials analysis [10] to nanotube based materials. Experimental realization of ion channeling through nanotubes is still at the preliminary stage [11, 12]. While the image force has not been found to play any significant role in channels of single crystals [10], its role has been identified clearly in ion-surface scattering [13], and in ion transmission through capillaries

in solids [14, 15]. In addition, although the image force plays a minor roles in ion channeling through nanotubes in the GeV and keV energy ranges [3, 2, 4, 16], it has been shown to strongly influence ion trajectories in the MeV energy range. For example, the image force gives rise to the rainbow effect in angular distributions of protons channeled through short chiral single-wall and double wall nanotubes [17].

It has been established that, when the nanotubes are grown in a dielectric medium, one may achieve a very high degree of ordering and straightening. This makes such composite structures very suitable candidates to be used in experiments of ion channeling through nanotubes. Therefore, it is important to study the effects of the surrounding dielectric medium on ion channeling through nanotubes in the MeV energy range. The materials of interest are Al_2O_3 [11], SiO_2 [18] as well as Ni [18] and Pt [12]. It has been shown recently that the image force and the rainbow effect in the angular distributions of protons channeled through nanotubes may be strongly modified by the polarization of the surrounding cylindrical dielectric boundary [19, 20, 21].

2. Theory

The system under investigation is a proton moving through an (11, 9) single-wall carbon nanotube embedded in a dielectric medium. The z axis coincides with the nanotube axis and the origin lies at its transverse entrance plane. The initial proton velocity is taken to be parallel to the z axis. We assume that the nanotube is sufficiently short for the proton energy loss to be neglected. The initial proton speed, v, is varied between 3 and 10 a.u., corresponding to energies between 0.223 and 2.49 MeV, respectively. The nanotube length, L, is varied between 0.1 and 1.0 μm.

We assume that the (repulsive) interaction between the proton and nanotube atoms may be treated classically using the Doyle-Turner expression for the proton-nanotube atom interaction potential averaged axially and azimuthally [23, 24, 25]. The resulting interaction potential may be expressed as

$$U_{rep}(r) = \frac{16\pi Z_1 Z_2 d}{3\sqrt{3}l^2} \sum_{j=1}^{4} a_j b_j^2 I_0(b_j^2 r d) \exp\{-b_j^2[r^2 + (d/2)^2]\}. \quad (1)$$

Here $Z_1 = 1$ and $Z_2 = 6$ are the atomic numbers of the proton and nanotube atom, respectively, d is the nanotube diameter, l is the bond length for nanotube atoms, r is the distance between the proton and nanotube axis, I_0 designates the modified Bessel function of the first kind and the 0^{th} order, and $a_j = (0.115, 0.188, 0.072, 0.020)$ and $b_j = (0.547, 0.989, 1.982, 5.656)$ are fitting parameters [25].

The dynamic polarization of the nanotube and dielectric medium by the proton is treated using a two-dimensional hydrodynamic model for the valence electrons of the nanotube atoms. This is based on a jellium-like description of the nanotube ion cores, extended to include the contribution of the dielectric boundary [20, 21, 26, 27]. This model includes the procedures of axial and azimuthal averaging, used in the repulsive interaction model. It gives the (attractive) interaction potential between the proton and its image. The image interaction potential at the proton position is then $U_{atr} = -\frac{Z_1}{2}\Phi_{ind}(\vec{r}, t)$, where $\Phi_{ind}(\vec{r}, t)$ is the electric potential at the proton position due to polarization charges induced on the nanotube and dielectric boundary by the (screened) proton. This is called the induced potential. A more detailed description of the theoretical hydrodynamic model is given in Refs. [19] and [20].

The total interaction potential between the proton and the nanotube and dielectric medium is $U(\vec{r}, t) = U_{rep}(r) - \frac{Z_1}{2}\Phi_{ind}(\vec{r}, t)$. The angular and spatial distributions of channeled protons in the exit plane are generated using a computer simulation method, which includes the numerical solving of the proton equations of motion in the transverse plane. The rectangular coordinates

of the initial proton position, x_0 and y_0, are chosen randomly from a two-dimensional uniform distribution under the condition $r_0 = (x_0^2 + y_0^2)^{\frac{1}{2}} < a - a_{sc}$, where $a_{sc} = \left[9\pi^2/(128\ Z_2)\right]^{\frac{1}{3}} a_0$ is the nanotube atom screening radius and a_0 the Bohr radius. We take for the nanotube atom bond length $l = 0.144$ nm [28] and obtain for the nanotube radius $a = 0.689$ nm. The initial number of protons is 3 141 929.

Angular distributions may be analyzed successfully via the corresponding mapping of the impact parameter plane to the scattering angle plane [5, 6, 7, 8, 17, 29]. We also analyze the mapping of the entrance transverse plane to the exit transverse plane. However, since in the case we investigate the total interaction potential is axially symmetric, it is possible to construct the one dimensional deflection function, Θ_x as a function of x_0 for the angular distribution. In the configuration plane we can analyze the mapping of the proton radial axis in the entrance transverse plane x_0 to the proton radial axis in the exit transverse plane x ($x_0 \mapsto x$). The extrema in this mapping are the rainbow maxima or minima, and the corresponding singularities in the angular and spatial distribution of channeled protons are the rainbow singularities.

3. Results and discussion

We use for the nanotube radius $a = 13.01$ a.u, and for the separation between the nanotube and the dielectric boundaries 3.21 a.u. [22, 30]. Thus, the dielectric boundary radius is $b = a + 3.21$ a.u. We describe the surrounding SiO_2 using a dielectric constant of 3.9 [31]. The dielectric responses of the surrounding Al_2O_3 and Ni are modeled using the methods described by Arista and Fuentes [15] and Kwei et al. [32], respectively. We have found that for the case of nanotube embedded in a dielectric media a proton moving at a speed below about 3 a.u. does not polarize the dielectric media. This means that the dielectric medium is completely screened by the nanotube and does not contribute to the image force. For a proton speed above about 3 a.u., polarization of the dielectric media occurs. The screening of the dielectric medium by the nanotube is then incomplete and it thus influences the image force.

Figure 1(a) shows two angular distributions of channeled protons along the Θ_x axis for $v = 3$ a.u. and $L = 0.3$ μm, both with and without the inclusion of the dynamical polarization effect. One can see that 10 maxima appear in the angular distribution, located around 10 scattering angles, $\Theta_x \cong \pm\ 0.7$ mrad, $\pm$ 1.1 mrad, $\pm$ 1.8 mrad, $\pm$ 2.1 mrad, $\pm$ 2.3 mrad, when the dynamical polarization effect is included. The extremal points are labeled by 1, $2'$, $2''$, $3'$ and $3''$, which result from one (1), two ($2'$ and $2''$) and three ($3'$ and $3''$) deflections of the rainbow trajectories within the image-generated potential well. Figure 1(b) shows two deflection functions that correspond to the angular distributions shown in Figure 1(a). The deflection function with the inclusion of the dynamical polarization effect has 10 extremum points: five minima and five maxima, which are designated by 1, $2'$, $2''$, $3'$ and $3''$. In both cases we notice two additional pairs of extrema near the nanotube wall (for large impact parameters), but these structures are not visible in the angular distributions. Figure 1(c) shows two spatial distributions of channeled protons along the x axis in the exit plane for the proton velocity $v = 3$ a.u. and the nanotube length $L = 0.3$ μm. The nanotube is placed in vacuum. The spatial distributions correspond to the cases when the image interaction potential is neglected and when it is included. In the former case the spatial distribution contains a central maximum and three pairs of peripheral maxima, designated by 1, 2 and 3, located at $x = \pm 7.5$, ± 11.1 and ± 12.1 a.u. In the latter case a central maximum and five pairs of peripheral maxima are seen, designated by 1_i, 2_i, 3_i, 4_i and 5_i, and located at $x = \pm 8.1$, ± 9.9, ± 10.7, ± 11.4 and ± 12.2 a.u. The maxima designated by 2, 3, 4_i and 5_i are very weak. When the image interaction potential is included, the central maximum is much narrower and about three times weaker while the peripheral maxima are much more prominent. Figure 1(d) shows two mappings of the x_0 axis in the entrance plane to the x axis in the exit plane corresponding to the two spatial distributions of channeled protons shown in Fig. 1(c). It is evident that without the image force the mapping has six extrema, three maxima

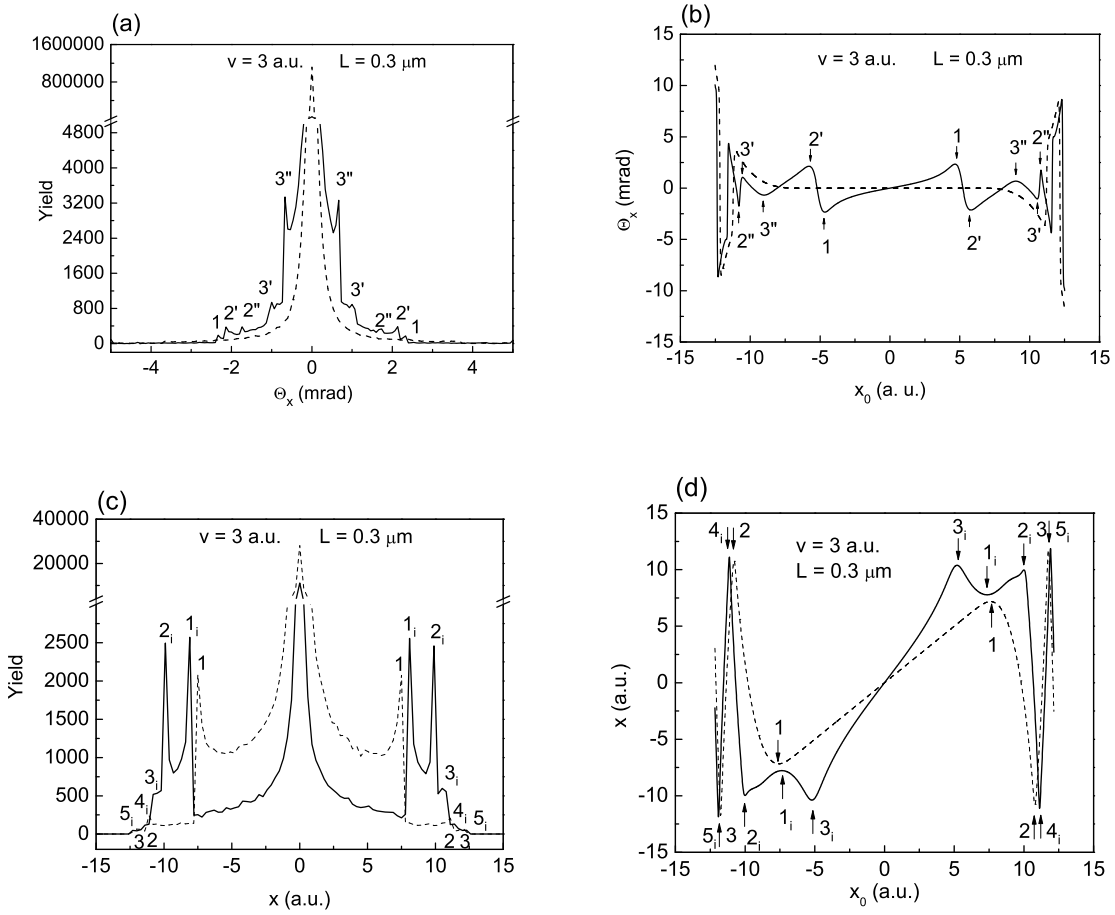

Figure 1. (a) Two angular distributions and (b) two corresponding deflection functions, (c) two spatial distributions and (d) two corresponding mapping $x_0 \mapsto x$ of channeled protons for the proton speed of 3 a.u. and the nanotube length of 0.3 μm. The (11, 9) SWNT is placed in vacuum. The dashed line corresponds to the case without the dynamic polarization effect and the solid line to the case with it.

and three minima. These are designated by 1, 2 and 3. When the image force is included, the mapping has 10 extrema, five maxima and five minima. These are designated by 1_i, 2_i, 3_i, 4_i and 5_i. The maxima and minima designated by 2, 3, 4_i and 5_i are very sharp and lie near the nanotube wall.

Figure 2(a) shows two angular distributions of channeled protons along the Θ_x axis in the scattering plane for the proton speed $v = 5$ a.u. and the nanotube length $L = 0.5$ μm. These correspond to the cases in which the nanotube is placed in vacuum and embedded in SiO_2, and the dynamic polarization effect is included. We notice a significant depletion of the number of rainbow peaks, down to three pairs (1, 2′ and 2″) for the nanotube in vacuum, and only one pair (1_d) for surrounding SiO_2. When the nanotube is placed in vacuum the peripheral maxima are located at $\Theta_x = \pm 0.23$, ± 0.43 and ± 0.74 mrad, and when it is embedded in SiO_2 at $\Theta_x = \pm 0.43$ mrad. Figure 2(b) shows two deflection functions that correspond to the angular distributions shown in Figure 2(a). In both cases we notice two additional pairs of extrema near the nanotube wall, but these structures are not visible in the angular distributions. Figure 2(c) shows two spatial distributions of channeled protons along the x axis in the exit plane for the proton speed $v = 5$ a.u. and the nanotube length $L = 0.5$ μm. These correspond to when the nanotube is

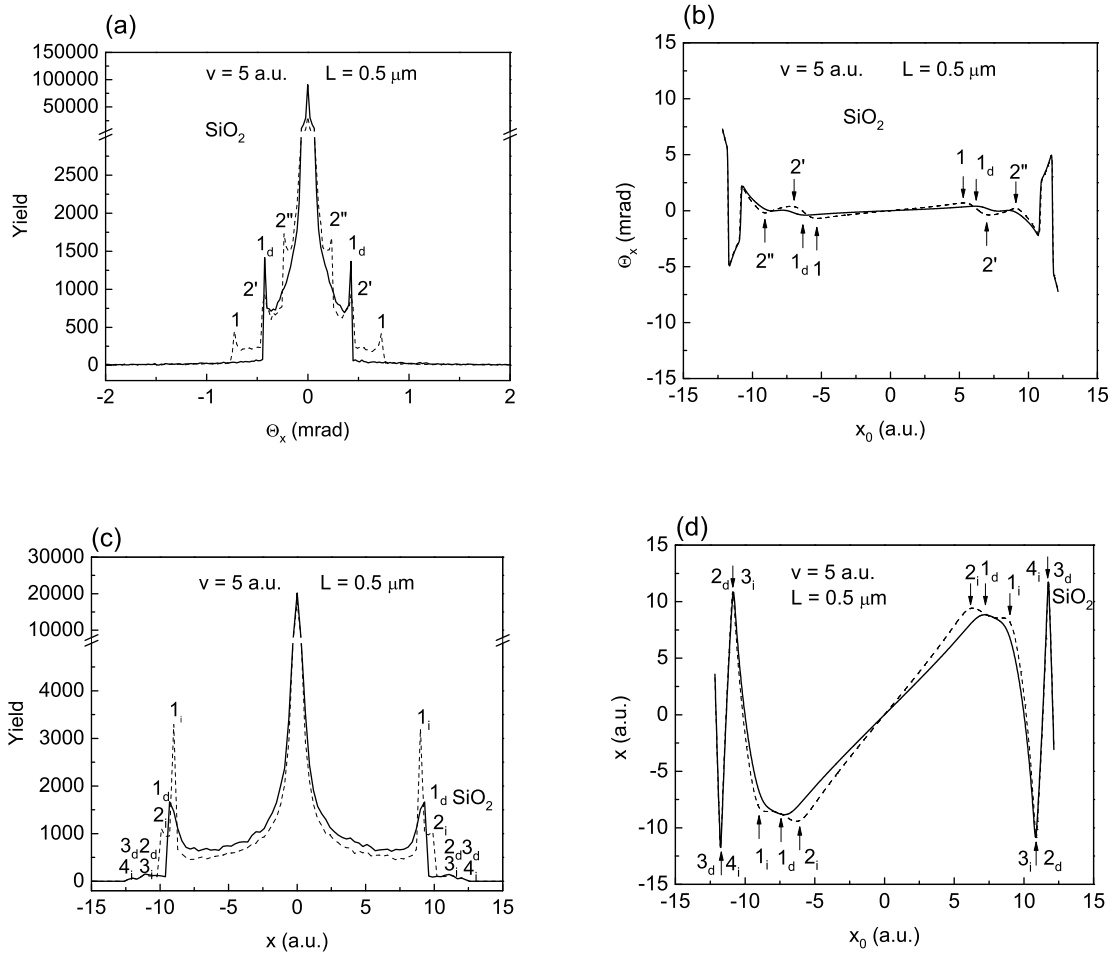

Figure 2. (a) Two angular distributions and (b) two corresponding deflection functions, (c) two spatial distributions and (d) two corresponding mapping $x_0 \mapsto x$ of channeled protons for the proton speed of 5 a.u. and the nanotube length of 0.5 μm. The (11, 9) SWNT is placed in vacuum (dashed line) and in SiO_2 (solid line).

placed in vacuum and embedded in SiO_2, with the dynamic polarization effect included. In the former case the spatial distribution contains a central maximum and four pairs of peripheral maxima are seen, designated by 1_i, 2_i, 3_i and 4_i. In the latter case a central maximum and three pairs of peripheral maxima, designated by 1_d, 2_d and 3_d. The maxima designated by 3_i, 4_i, 2_d and 3_d are very weak. When the nanotube is placed in vacuum the peripheral maxima are located at $x = \pm 9.0$, ± 9.9, ± 11.2 and ± 12.1 a.u., and when it is embedded in SiO_2 at $x = \pm 9.3$, ± 11.2 and ± 12.1 a.u. Figure 2(d) shows two mappings of the x_0 axis in the entrance plane to the x axis in the exit plane corresponding to the two spatial distributions of channeled protons shown in Fig. 2(c). It is evident that when the nanotube is placed in vacuum the mapping has eight extrema, four maxima and four minima. These are designated by 1_i, 2_i, 3_i and 4_i. When the nanotube is embedded in SiO_2 the mapping has six extrema, three maxima and three minima. These are designated by 1_d, 2_d and 3_d.

Figure 3(a) shows four angular distributions of channeled protons along the Θ_x axis in the scattering angle plane for the proton speed $v = 8$ a.u. and the nanotube length $L = 0.8$ μm. These correspond to when the nanotube is placed in vacuum and embedded in SiO_2, Al_2O_3 and Ni, with the image interaction potential included. One notices that the positions of the

rainbow extrema, labeled by 1_d, hardly change for different dielectrics. When the nanotube is placed in vacuum there are no peripheral maxima, and when it is embedded in a dielectric medium, periferal maxima are located at $\Theta_x = \pm 0.17$ mrad (in the case of Al_2O_3) and $\Theta_x = \pm 0.21$ mrad (in the cases of SiO_2 and Ni). Figure 3(b) shows four deflection functions that correspond to the angular distributions shown in Fig. 3(a). One finds that in each case of the nanotube embeded in a dielectric the mapping has one pair of extrema, labeled by 1_d. In both cases we notice two additional pairs of extrema near the nanotube wall which are not visible in the angular distributions. Figure 3(c) shows four spatial distributions of channeled protons along the x axis in the exit plane for the proton speed $v = 8$ a.u. and the nanotube length $L = 0.8$ μm. These correspond to the cases in which the nanotube is placed in vacuum and embedded in SiO_2, Al_2O_3 and Ni, with the image interaction potential is included. In each case the spatial distribution contains a strong central maximum and three pairs of peripheral maxima, designated by 1_i, 2_i and 3_i, when the nanotube is placed in vacuum, and by 1_d, 2_d and 3_d, when it is embedded in SiO_2,Al_2O_3 and Ni. It is clear that the spatial distributions when the nanotube is embedded in the three dielectric media are very similar to each other. Also, they do not differ significantly from the spatial distribution when the nanotube is placed in vacuum. The spatial distributions when the nanotube is embedded in SiO_2 and Ni almost coincide. Figure 3(d) shows four mappings of the x_0 axis in the entrance plane to the x axis in the exit plane corresponding to the four spatial distributions of channeled protons shown in Fig. 3(c). One finds that in each case the mapping has six extrema, three maxima and three minima.

All angular and spatial distributions shown are characterized by the same duration of the proton channeling process, i.e., by the same proton dwell time.

The results for the angular distributions for the combination of parameters $L = 0.3$ μm and v= 3 a.u. are displayed in Fig. 1(a), where one can see five pairs of the extremal points, labeled by 1, $2'$, $2''$, $3'$ and $3''$. For the combination of parameters $L = 0.5$ μm, v= 5 a.u. (see Fig. 2(a)), one notices a significant depletion of the number of rainbow peaks, down to three pairs (1, $2'$ and $2''$) for the nanotube in vacuum, and only one pair (1_d) for surrounding SiO_2. The further reduction of the number of rainbow peaks with increasing proton speed is illustrated in Fig. 3(a) for the combination of parameters $L = 0.8$ μm, v= 8 a.u. This is due to the diminished image force on protons at such a high speed. On the other hand, the one rainbow peak (1_d) from Fig. 2(a) has remained in Fig. 3(a) for the case of a nanotube surrounded by SiO_2, although this peak is now very small. This persistence of the rainbow peak for a surrounding dielectric can be explained by the "transparency" of nanotubes at high proton speeds [26], where the image force is dominated by the polarization of the surrounding dielectric.

For $v = 3$ a.u. and $L = 0.3$ μm, the spatial distribution with the nanotube placed in vacuum contains five rainbow maxima [see Fig. 1(c)], as does the spatial distribution with the nanotube placed in SiO_2. For $v = 5$ a.u. and $L = 0.5$ μm the spatial distribution with the nanotube placed in vacuum contains four rainbow maxima, while the spatial distribution with the nanotube placed in SiO_2 three rainbow maxima [see Fig. 2(c)]. For $v = 8$ a.u. and $L = 0.8$ μm the spatial distribution with the nanotube placed in vacuum contains three rainbow maxima, as does the spatial distribution with the nanotube placed in SiO_2 [see Fig. 3(c)]. It is clear that for the same proton dwell time the number of rainbow maxima in the spatial distribution decreases with the proton speed.

4. Conclusions

We have presented theoretical investigations of the effects of dynamic polarization of the nanotube atom valence electrons on the angular and spatial distributions of protons channeled through (11, 9) single-wall carbon nanotubes placed in vacuum and embedded in various dielectric media, for proton speeds between 3 and 10 a.u. and nanotube lengths between

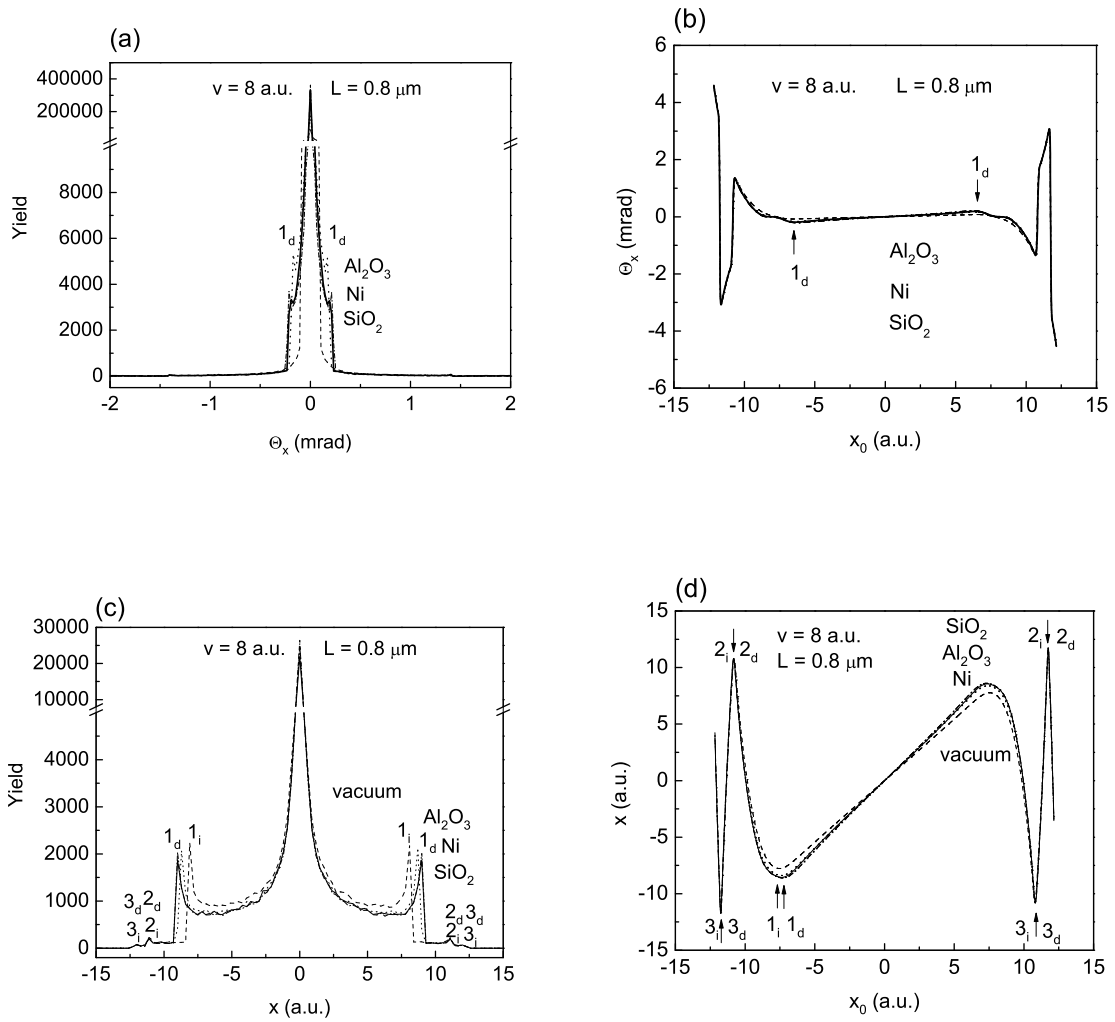

Figure 3. (a) Four angular distributions and (b) four corresponding deflection functions, (c) four spatial distributions and (d) four corresponding mapping $x_0 \mapsto x$ of channeled protons for the proton speed of 8 a.u. and the nanotube length of 0.8 μm. The (11, 9) SWNT is placed in vacuum (dashed line) and in SiO_2, Al_2O_3 and Ni (solid, dotted and dash-dotted lines, respectively).

0.1 and 1.0 μm. We found that the image force gives rise to the rainbow effect, which may be strongly affected by the surrounding dielectric medium for proton speeds above 3 a.u. Our study has revealed that prominent rainbow maxima exist in the angular and spatial distributions of channeled protons. While the rainbows in the angular distributions of channeled ions may be easily measured and used to provide information on the structure and atomic forces inside the nanotubes, the rainbows in the spatial distributions of channeled ions may be employed for detecting and locating the atoms and molecules intercalated in the nanotubes.

We also find prominent peripheral maxima in the spatial distributions at the distances from the nanotube wall on the order of a few tenths of a nanometer. These distances are suitable for applying proton channeling to probe the atoms and molecules adsorbed on the nanotube wall. We have revealed that the image force is responsible for the appearance of additional prominent peripheral maxima as well as for making them more prominent at the expense of the central maximum, as the nanotube length increases in angular and spatial distributions.

All our findings indicate that it is important to carefully consider in future simulations and experiments the role played by dielectric media in ion channeling through carbon nanotubes in the MeV energy range. Such studies may further elucidate dielectric properties of carbon nanotubes in the presence of dielectric media of relevance to nanoelectronics, such as SiO_2. The spatial distribution of channeled protons gives us detailed information about the proton flux within the nanotube. It appears that a careful studying of the speed dependence of the image force as well as of the properties of the nanotube and its surroundings, may help us better understand and perhaps even find a way to induce a spatial redistribution of channeled protons towards the nanotube wall. Redistributing channeled protons might then be used for probing the atoms and molecules intercalated in the nanotube. We also mention the possibility of producing nanosized ion beams with nanotubes embedded in various dielectric media for applications in biomedical research.

References

[1] Mišković Z L 2007 *Radiation Effects and Defects in Solids* **162**, 185
[2] Artru X, Fomin S P, Shulga N F, Ispirian K A and Zhevago N K 2005 *Phys. Rep.* **412** 89
[3] Moura C S, Amaral L 2007 Carbon 45 1802; 2005 *J. Phys. Chem.* B **109** 13515
[4] Biryukov V M and Bellucci S 2005 *Nucl. Instrum. Meth. Phys. Res.* B **230** 619
[5] Petrović S, Borka D and Nešković N 2005 *Eur. Phys. J.* B **44** 41
[6] Petrović S, Borka D and Nešković N 2005 *Nucl. Instrum. Meth. Phys. Res.* B **234** 78
[7] Borka D, Petrović S and Nešković N 2005 *Mat. Sci. For.* **494** 89
[8] Nešković N, Petrović S and Borka D 2005 *Nucl. Instrum. Meth. Phys. Res.* B **230** 106
[9] Bellucci S, Biryukov V M, Chesnokov Y A, Guidi V and Scandale W 2003 *Phys. Rev.* ST AB **6** 033502
[10] Feldman L C, Mayer J W and Picraux S T 1982 *Materials Analysis by Ion Channeling* (Academic Press, New York)
[11] Zhu Z, Zhu D, Lu R, Xu Z, Zhang W and Xia H 2005 *Proc. Of SPIE* Vol. **5974** Bellingham, WA 597-1
[12] Chai G, Heinrich H, Chow L and Schenkel T 2007, *Appl. Phys. Lett.* **91** 103101
[13] Winter H 2002 *Phys. Rep.* **367** 387
[14] Arista N R 2001 *Phys. Rev.* A **64** 32901; Arista N R and Fuentes M A 2001 *Phys. Rev.* B **63** 165401
[15] Tökési K, Tong X M, Lemell C and Burgdörfer J 2005 *Phys. Rev.* A **72** 022901
[16] Krasheninnikov A V and Nordlund K 2005 *Phys. Rev.* B **71** 245408
[17] Borka D, Petrović S, Nešković N, Mowbray D J and Mišković Z L 2006 *Phys. Rev.* A **73** 062902; 2007 *Nucl. Instrum. Meth. Phys. Res.* B **256** 131
[18] Guerret-Plécourt C, Le Bourar Y, Loiseau A and Pascard H 1994 *Nature* **372** 761
[19] Mowbray D J, Mišković Z L and Goodman F O 2006 Phys. Rev. B **74** 195435
[20] Borka D, Mowbray D J, Mišković Z L, Petrović S and Nešković N 2008 *Phys. Rev.* A **77** 032903
[21] Borka D, Mowbray D J, Mišković Z L, Petrović S and Nešković N 2008 Jour. Phys. Con. Mett., in press.
[22] Hulman M, Kuzmany H, Dubay O, Kresse G, Li L, Tang Z K, Knoll P and Kaindl R 2004 *Carbon* **42** 1071
[23] Lindhard J 1965 *K. Dan. Vidensk. Selsk., Mat.-Fys. Medd.* **34** 1
[24] Zhevago N K and Glebov V I 1998 *Phys. Lett.* A **250** 360; 2000 *J. Exp. Theor. Phys.* **91** 504
[25] Doyle P A and Turner P S 1968 *Acta Crystallogr.* A **24** 390
[26] Doerr T P and Yu Y-K 2004 *Am. J. Phys.* **72** 190
[27] Mowbray D J, Mišković Z L, Goodman F O and Wang Y-N 2004 *Phys. Rev.* B **70** 195418
[28] Saito R, Dresselhaus G, Dresselhaus M S 2001 *Physical Properties of Carbon Nanotubes* (Imperial College Press, London)
[29] Berdinsky A S, Alegaonkar P S, Lee H C, Jung J S, Han J H, Yoo J B Fink D and Chadderton L T 2007 *Nano* **2** 59
[30] Soler J M, Artacho E, Gale J D, García A, Junquera J, Ordejón P and Sánchez-Portal D 2002 *J. Phys. Condens. Matter* **14** 2745
[31] Swart J W, Diniz J A, Doi I and de Moraes M A B 2000 *Nucl. Instrum. Meth. Phys. Res.* B **166-167** 171
[32] Kwei C M, Chen Y F, Tung C J and Wang J P 1993 *Surf. Sci* **293**, **3** 202